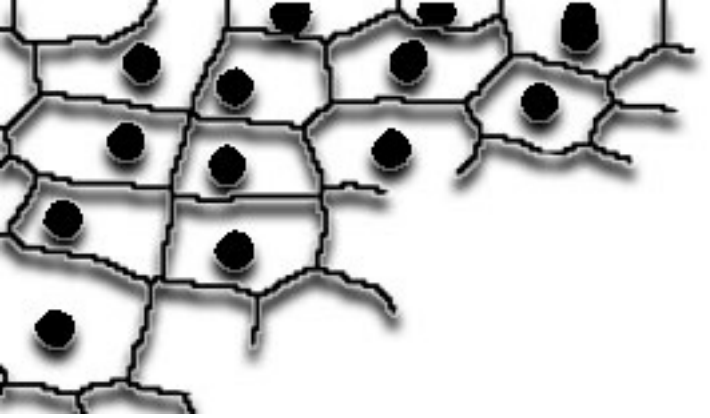

2

RPTPα and PTPε Signaling via Fyn/Yes and RhoA is Essential for Zebrafish Convergence and Extension Cell Movements during Gastrulation

Mark van Eekelen*, Vincent Runtuwene*, John Overvoorde, Jeroen den Hertog

Dev Biol. 2010 Apr 15;340(2):626-39

*=equal contribution

Abstract

Convergence and extension (C&E) cell movements are essential to shape the body axis during vertebrate gastrulation. We have used the zebrafish to assess the role of the receptor protein-tyrosine phosphatases, RPTPα and PTPε, in gastrulation cell movements. Both RPTPα and PTPε knockdown and *ptpra−/−* embryos show defects in C&E movements. A method was developed to track gastrulation cell movements using confocal microscopy in a quantitative manner and *ptpra−/−* embryos displayed reduced convergence as well as extension speeds. RPTPα and PTPε knockdowns cooperated with knockdown of a well known factor in C&E cell movement, non-canonical Wnt11. RPTPα and PTPε dephosphorylate and activate Src family kinases in various cell types *in vitro* and *in vivo*. We found that Src family kinase phosphorylation was enhanced in *ptpra−/−* embryos, consistent with reduced Src family kinase activity. Importantly, both *ptpra−/−* and RPTPα and PTPε knockdown induced C&E defects were rescued by active Fyn and Yes. Moreover, active RhoA rescued the RPTPα and PTPε knockdown and *ptpra−/−* induced gastrulation cell movement defects as well. Our results demonstrate that RPTPα and PTPε are essential for C&E movements in a signaling pathway parallel to non-canonical Wnts and upstream of Fyn, Yes and RhoA.

Introduction

RPTPα (*ptpra*) and PTPε (*ptpre*) are two highly similar receptor-like protein-tyrosine phosphatases consisting of a short highly glycosylated extracellular domain and two cytoplasmically localized phosphatase domains. RPTPα and PTPε are involved in several processes, including cell polarization (Chiusaroli et al., 2004; Herrera Abreu et al., 2008), migration (Zeng et al., 2003) and cell cycle control (Ardini et al., 2000). The function of RPTPα and PTPε is often ascribed to direct activation of Src family kinases (SFKs) through dephosphorylation of the inhibitory pTyr527 residue in the C-terminus (Courtneidge, 1985; den Hertog et al., 1993; Peretz et al., 2000; Zheng et al., 1992). Src and SFKs are known to be activated by different stimuli, including cell adhesion to ECM proteins and growth factors (Hsia et al., 2005; Roche et al., 1995). Many of these actions require actin cytoskeleton remodeling through activation of Rho GTPase family members (Ridley and Hall, 1992; Ridley et al., 1992).

During vertebrate gastrulation a series of cellular movements result in the formation of the three germ layers, endoderm, mesoderm and ectoderm that create the basic body plan of the developing embryo (Warga and Kimmel, 1990). Convergence and extension (C&E) represent two of these essential cell movements that have been well characterized in zebrafish. Cells converge towards the midline, forming the medial/lateral axis, where they intercalate with one another

and extend around the yolk, giving rise to the anterior/posterior axis (Griffin et al., 1995; Keller et al., 1992; Solnica-Krezel et al., 1996). C&E cell movements are regulated by the non-canonical Wnt signaling pathway which is similar to the planar cell polarity (PCP) pathway identified in *Drosophila* (Matsui et al., 2005; Medina et al., 2000; Solnica-Krezel and Eaton, 2003).

In vertebrates, the non-canonical Wnt pathway becomes activated when Wnt11 or Wnt5 binds to Frizzled receptors resulting in the downstream activation of RhoA and Rac. RhoA and Rac subsequently propagate the signal to their respective downstream effectors, including Rok2 and JNK (Habas et al., 2003, 2001; Veeman et al., 2003). In *C. elegans*, this cascade will remodel the cell, establishing polarity and allowing it to mount a proper chemotactic response through remodeling of the actin cytoskeleton (Goldstein et al., 2006). It is assumed that non-canonical Wnt signaling induced cell polarization is at the basis of vertebrate C&E cell movements as well. A number of mutants have been described in zebrafish that harbor mutations in genes regulating this process (Heisenberg et al., 2000; Jessen et al., 2002; Kilian et al., 2003; Topczewski et al., 2001). The phenotype that all of these mutants have in common is that the embryos are shorter and broader as one might expect if C&E are disrupted.

More recently a number of studies have come to light that show that C&E is not solely governed by the non-canonical Wnt pathway. The list of other factors that modulate non-canonical Wnt signaling directly (Wada et al., 2005) or function independently (Hannus et al., 2002) is ever growing. Recently, we have shown that signaling through the Src family kinases Fyn and Yes converges with noncanonical Wnt signaling and serves to modulate the activity of the small GTPase RhoA during C&E cell movements (Jopling and den Hertog, 2005).Csk, a negative regulator of SFKs also has a role in C&E cell movements (Jopling and den Hertog, 2007). Moreover, we have shown that the protein-tyrosine phosphatase Shp2, an indirect activator of SFKs (Zhang et al., 2004), regulates C&E during gastrulation via Fyn/Yes and RhoA (Jopling et al., 2007).

Here we show that knockdown of RPTPα or PTPε induced C&E defects using *in situ* hybridization of C&E specific markers. Coinjection of ptpra-MO and ptpre-MO induced various degrees of cyclopia in fish, indicating that RPTPα and PTPε are at least partially redundant. *Ptpra* mutant zebrafish were isolated by target selected gene inactivation and we established that *ptpra−/−* embryos displayed C&E defects, similar to the ptpra-MO injected embryos. Time-lapse confocal microscopy was used to track cell movements during gastrulation and this technology was adapted to allow quantification of cell movements during gastrulation. *Ptpra−/−* embryos displayed reduced C&E cell movement speed as compared to wildtype siblings. Co-injection of low amounts of ptpra-MO or ptpre-MO together with low amounts of Wnt11-MO phenocopied the silberblick phenotype,

suggesting that RPTPα and PTPε have a genetic interaction with Wnt11. In search of an underlying mechanism, we found enhanced SFK phosphorylation on the inhibitory site and reduced SFK autophosphorylation, indicating that SFK activity was reduced in mutant embryos compared to siblings. C&E defects in *ptpra−/−* embryos were rescued by active Fyn and Yes, which is consistent with RPTPα being upstream of SFKs. Moreover, active RhoA rescued the *ptpra−/−* phenotype as well. Based on our data, we propose a model in which RPTPα and PTPε act in parallel to non-canonical Wnt signaling upstream of the SFKs, Fyn and Yes and upstream of RhoA.

Materials and methods

Zebrafish and in situ hybridization

Zebrafish were kept and the embryos were staged as described before (Westerfield, 1995). *In situ* hybridizations were done essentially as described (Thisse et al., 1993) using probes specific for *bmp2b, chd, gsc, ntla, dlx3, hgg1* (currently known as *ctsl1b*), *myod* and *krox20* as described (Jopling and Hertog, 2007; Jopling et al., 2007). *In situ* probes for *ptpra*, *ptprea* and *ptpreb* were generated by performing an RT reaction on isolated RNA from zebrafish embryos (48 hpf). We designed oligos to perform PCR on the cDNA constructs of *ptpra*, *ptprea* and *ptpreb* spanning approximately 800 bp, and a nested oligo pair with a T7 sequence in the reverse oligo. We used the T7 tag to generate DIG labeled antisense RNA for *in situ* hybridization and the nested oligo pair to verify the sequences. A premature stop *ptpra* mutant was identified using target selected gene inactivation as described in Wienholds et al. (2002). The *ptpra*^{hu3334} allele changes a TTG to a TAG codon resulting in a L133STOP coding change.

Constructs

Mouse *ptpra* constructs were used as described earlier (den Hertog and Hunter, 1996). For zebrafish *ptpra* contructs 1 dpf zebrafish were lysed and mRNA was isolated. Reverse transcription was done with oligo dT and *ptpra* cDNA was amplified and cloned into a pSG5-13 vector and sequenced.

MOs, RNA and injections

Antisense splice site donor MOs were designed one or two exons upstream of the catalytic site of the respective cDNAs and ordered from GeneTools (Philomath,OR): ptpra, 5′-TTGCGGCGTTTACCTCTTTCCGCTC; ptprea, 5′-AAGGGATGCTAACCTCTTTTCTCTC; ptpreb, 5′ TATCTTATCTCACCTCTTTTCTCTC; wnt11 as described in: Lele et al. (2001). 5′ capped sense RNAs were synthesized using mMessage mMachine kit (Ambion). The amount of RNA that was injected at the one cell stage was optimized for each synthetic RNA. For the rescue experi-

ments, we used mutant, constitutively active forms of human Fyn, Yes (Jopling and denHertog, 2007), and active human RhoA and Rac1 (Jopling and den Hertog, 2005) as described previously. Phenotypes were assessed at indicated stages, based on morphology or based on *dlx3*/*hgg1* markers at 10 hpf.

Western blot

Embryos were grown until 52 hpf and were deyolked with deyolking buffer (1/2 Ginzburg Fish Ringer) without calcium (Link et al., 2006; Westerfield, 1995). Subsequently embryos were grinded in buffer containing 50 mM Tris, pH 7.5, 150 mM NaCl, 1 mM EDTA, 1 mM sodium orthovanadate, 1% Nonidet P-40, 0.1% sodium deoxycholate, and protease inhibitor mixture (Complete Mini, Roche Diagnostics) and lysed using a syringe. Lysates were centrifuged at 14,000 g to pellet cellular debris. Lysates were subjected to SDS-PAGE and blotted (amount loaded per lane corresponds to 15 embryos). After transfer the membrane was stained with Coomassie Blue stain to verify equal loading of the lysates. Subsequently the PVDF membrane was blocked with 1% BSA or 5% Milk and then incubated with the corresponding antibodies against pSrc418 (1:1000, BioSource Technologies), actin (1:5000, kindly provided by MP Peppelenbosch, University Medical Center Groningen, the Netherlands) and antiserum against RPTPα#5478 (1:1000; den Hertog et al., 1994) followed by the horseradish peroxidase conjugated secondary antibody. The membranes were subjected to detection by enhanced chemiluminescence.

Confocal microscopy

Histone 1 injection

The embryos were injected at the 1-cell stage with Histone 1 tagged with Alexa fluor 488 from Molecular Probes (H1).

Image acquisition

For time-lapse imaging the embryos were dechorionated (at 30% epiboly) and mounted at shield stage in 1% low melting point agarose in E3 embryo rearing medium and covered with E3 in a culture dish with a glass coverslip replacing the bottom. A Leica SP2 confocal microscope with a 40x objective was used for live imaging of the Alexa 488 signal using a 488 nm laser line for excitation. Temperature was maintained at approximately 28.5 °C on a heated stage. Time points were recorded every 2 min from shield stage until 1-somite stage.

Positioning

The H1-injected embryos are positioned with the dorsal side against the coverslip approximately 100 μm anterior to shield position. At this position the

C&E cell movements of the epiblast can be clearly visualized.

Analysis

Time-lapse images were analyzed using ImageJ (http://rsbweb.nih.gov/ij/). The nuclear labeling is used to determine the position of the individual cells in a single optical slice for each time point. In the images the embryo is positioned with the anterior side towards the top of the image. The Cartesian coordinates of cell tracks generated in this way will represent the contribution of cell migration to convergence (X-axis) and extension (Y-axis).

Detection and tracing of cell positions

Due to the innate changes in intensity, size and shape of H1 signal of the nuclei additional image processing is needed for efficient tracing of the cells. Making the images binary solves the problem of variable fluorescent intensities. The occasionally occurring of fused objects is handled by a watershedding process which is able to reseparate most fused objects. These objects still change during the time-lapse run in size and shape. Eroding ever object to a single pixel generates an image with single point markings representing the individual positions of each object. For tracing purposes these single pixels need to be dilated. When the resulting image is re-projected onto the original it shows that the generated objects represent cell positions with a very high accuracy. The objects generated are readily traced with an algorithm plugin which implements the feature point detection and tracking algorithm as described in Sbalzarini and Koumoutsakos (2005). The algorithm generates a report with the Cartesian coordinates for all traced objects at each time point.

Quantification

During mid-gastrulation the general cell movements visualized with this method are in the extension direction. The Y-coordinates of the cell tracks are used as a measurement for the contribution of these cell tracks to extension of the embryo. The individual movements between time frames in the Y-direction of the traced cells are quantified. During late gastrulation the general cell movements visualized with this method are in the convergence direction. The X-coordinates of the cell tracks are used as a measurement for the contribution of these cell tracks to convergence of the embryo. The individual movements between time frames in the X-direction of the traced cells are quantified. The statistical analysis has been performed by the Microsoft Excel Student t-test assuming unequal variances with alpha=0.05.

Cell shape analysis

To achieve ubiquitous fluorescent membrane labeling, the embryos were

injected at 1 cell stage with 20 pg of mRNA encoding membrane-citrine (a YFP variant with a C-terminal fusion of the Ras membrane localization sequence [CAAX]). To visualize the cell shape in the presomitic mesoderm, membrane-citrine expressing live embryos were mounted in 0.75% soft agarose at the dorsal side in glass bottomed Petri dishes. Using a SP2 Leica confocal microscope the presomitic mesoderm was imaged using a 40x oil objective. Images were processed in ImageJ and, analysis of cell length-to-width ratio and angular deviation was performed by the Shape_Descriptor1u plugin (Syverud et al., 2007).

Results

Identification and expression of zebrafish ptpra, ptprea and ptpreb

To assess the function of *ptpra* and *ptpre* in early vertebrate development we set out to identify these genes in the zebrafish genome. We blasted the PTP domain of human RPTPα and PTPε respectively against the zebrafish genome Zv7 in the Ensembl database. Candidate gene hits were found based on homology of the PTP domain and similarity of the overall protein structure. They were blasted back against the human genome and aligned with RPTPα and PTPε of several species to validate these hits (Fig. 1), using Mega4 software (Tamura et al., 2007). Upon aligning it became apparent that the zebrafish genome contains one ortholog for RPTPα and two for PTPε, named PTPεa (*ptprea*) and PTPεb

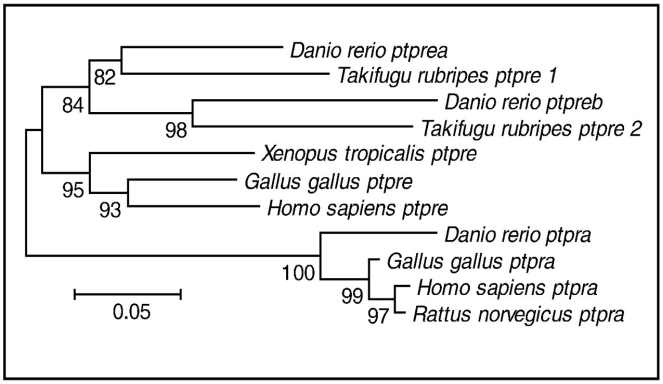

Fig. 1. RPTPα and PTPε are conserved in the zebrafish genome. Protein sequences were obtained from Ensembl database of RPTPα and PTPε from fugu, Xenopus, chicken and human. The N-terminal phosphatase domains were used to align with the zebrafish RPTPα and two PTPε (N-terminal phosphatase) protein sequences using the MEGA4 program. The evolutionary history was inferred using the Neighbor-Joining method.

The optimal tree with the sum of branch length = 0.96066757 is shown. The percentage of replicate trees in which the associated taxa clustered together in the bootstrap test (500 replicates) is shown next to the branches. The tree is drawn to scale, with branch lengths in the same units as those of the evolutionary distances used to infer the phylogenetic tree. The evolutionary distances were computed using the Dayhoff matrix based method and are in the units of the number of amino acid substitutions per site. All positions containing alignment gaps and missing data were eliminated only in pairwise sequence comparisons (pairwise deletion option). There were a total of 264 positions in the final dataset.

(*ptpreb*) henceforth. Zebrafish *ptpra* was found on chromosome 21 and annotated as ptpra (ENSDARG00000001769) and the coding sequence is consistent with the cDNA that we cloned previously (accession number Y15874) (van der Sar et al., 2002). *Ptprea* was found on chromosome 3, annotated as LOC567443 (ENSDARG00000015891); *ptpreb* was found on chromosome 17, annotated as NP_001038642.1 (ENSDARG00000021151). The zebrafish orthologs are highly homologous to human and mouse RPTPα and PTPε, showing 77%, 68% and 72% protein sequence identity to human and 75%, 71% and 72% protein sequence identity to mouse, respectively.

In order to reveal the expression patterns of *ptpra*, *ptprea* and *ptpreb* respectively, we generated *in situ* probes as described in the Materials and methods section. In short: a nested PCR was performed on a cDNA library to generate PCR products spanning approximately 800 bp of the *ptpra*, *ptprea* and *ptpreb* cDNAs and introducing a T7 tag for antisense RNA transcription on the 3′ end. The probes were verified by sequencing. *In situ* hybridization experiments show that *ptpra*, *ptprea* and *ptpreb* are ubiquitously expressed during early stages of zebrafish development (Fig. S1). At later stages (24 hpf, 36 hpf and 72 hpf) *ptpra*, *ptprea* and *ptpreb* are broadly expressed with enhanced levels of expression in the anterior parts of the embryo. The PCR products were verified by sequencing and since we detected mRNA expression of all three genes, we conclude that they all are functional genes.

RPTPα and PTPε knockdown induced C&E defects during gastrulation

In order to knockdown expression of RPTPα and PTPε, we designed splice donor MOs targeting the exon immediately upstream of the catalytic site of these genes and injected them at the one cell stage. We found that 0.3 ng ptpra-MO consistently produced specific defects in embryonic development. ptprea-MO or ptpreb-MO by themselves did not induce phenotypes, even at high concentrations. However, 2.5 ng ptprea-MO together with 2.5 ng ptpreb-MO induced specific defects, suggesting redundancy between the two *ptpre* genes. Henceforth, ptprea-MO and ptpreb-MO were co-injected and referred to as "ptpre-MOs". The earliest visible defect for both ptpra-MO and ptpre-MOs was at 10 hpf when the embryo fails to extend properly around the yolk. At later stages (2 dpf) the RPTPα knockdown and PTPε knockdown embryos were shorter and ptpra-MO injected embryos developed edemas around the heart and yolk (Figs. 2B, C). When co-injected, ptpra-MO and ptpre-MOs induced an increasingly severe phenotype even when lower amounts of morpholino were used. Occasionally, we observed a phenotype resembling the *silberblick* mutant phenotype (Heisenberg et al., 2000) and the Fyn/Yes knockdown phenotype (Jopling and den Hertog, 2005), with a subset of fish showing severe cyclopia (Figs. 2D–G). The phenotype was reminiscent of C&E defects and to verify that knockdown of RPTPα and PTPε affected

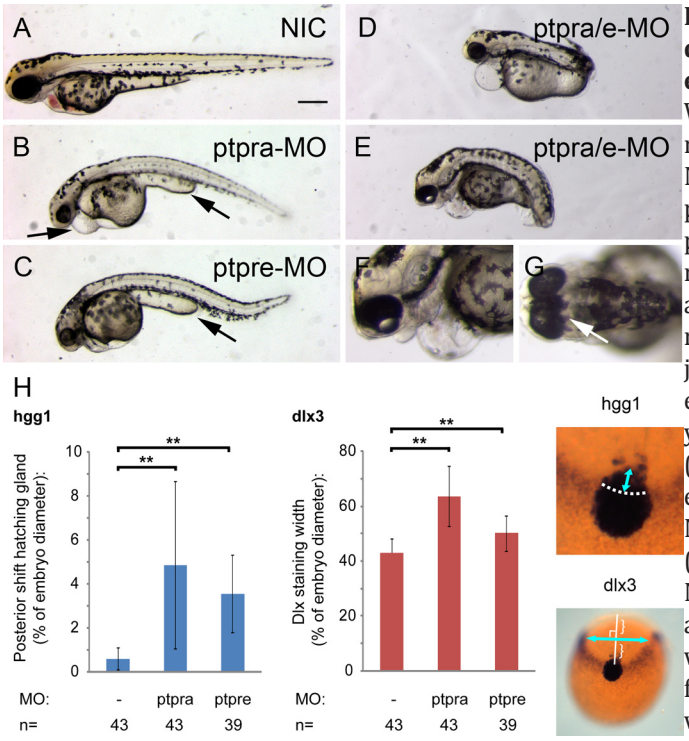

Fig. 2. RPTPα and PTPε knockdown fish show convergence and extension defects. Wildtype zebrafish embryos were micro-injected with 0.3 ng ptpra-MO (B), 2.5 ng ptprea-MO+ 2.5 ng ptpreb-MO(C) or triple injected with ptpra-MO (0.15 ng) and ptpre-MO (1 ng each, D–G) each at the 1 cell stage and grown to 48 hpf. Pictures show representative embryos. A non-injected embryo is included for reference (A). Arrows indicate shorter yolk extension (B, C), cardiac edema (B) or fused eyes (G). (H) Zebrafish embryos micro-injected with ptpra-MO (0.3 ng/embryo) or ptpre-MO (2.5 ng ptprea-MO+2.5 ng ptpreb-MO/embryo) at the one cell stage and non-injected control embryos were grown to 1 somite stage and fixed. Whole mount *in situ* staining was performed using probes for *dlx3* and *hgg1*. The resulting staining patterns were analyzed using ImageJ software, measuring the posterior shift of the *hgg1* staining as indicated in the panel on the right, and measuring the width of the *dlx3* staining half-way between the hatching gland and the edge of the embryo when seen from top view with the hatching gland positioned in the middle. The measured distances were plotted as the average posterior shift or width as a percentage of the total width of the embryo (yolk). Error bars indicate standard deviations, Student t-tests (2 tailed, assuming unequal variance) were performed between groups indicated, ** indicates a P-value<0.001. Scale bars=250 µm. *Dlx3/hgg1 in situ* data can be compared within experiments, but not between experiments because of subtle differences in experimental conditions. This experiment has been done at least three times. A representative experiment is depicted here.

C&E, morpholino injected embryos were fixed at the 1 somite stage and stained for *dlx3* (edges of the neural plate) and *ctsl1b* (referred to in this article as *hgg1*; precursor of the hatching gland) by whole mount *in situ* hybridization (Fig. 2H). C&E phenotypes were assessed by measuring the posterior shift of the hatching gland and the widening of the *dlx3* staining in injected and control embryos as indicated in the inset of Fig. 2H. The average lengths were plotted as a percentage of the embryo diameter and compared to control embryos by Student t-test. We found that knockdown of RPTPα or PTPε severely affected C&E movements (Fig. 2H).

In order to establish the effectiveness of the RPTPα knockdown, we analyzed RPTPα protein levels in zebrafish lysates by immunoblotting with an immunoserum against mouse RPTPα. We found that ptpra-MO reduced RPTPα protein expression in a dose-dependent manner (Fig. 3A). We proceeded to co-inject

morpholinos with varying amounts of RNA encoding mouse RPTPα or PTPε, which are not recognized by their respective morpholinos. RPTPα or PTPε RNA rescued the observed phenotypes when co-injected with ptpra-MO or ptpre-MO, respectively (Figs. 3B–D). Injection of RPTPα or PTPε RNA at these concentrations by itself did not affect early zebrafish development morphologically (data not shown). As a control, we co-injected similar amounts of GFP RNA, which did not rescue these phenotypes (Fig. S2). We conclude that the RPTPα and PTPε knockdowns were specific and induced phenotypes that were consistent with defects in C&E cell movements.

C&E defects in ptpra−/− zebrafish embryos

In search of genetic mutants that lack functional RPTPα, we used target selected gene inactivation (Wienholds et al., 2002) and identified a nonsense mutation in exon 3 of ptpra. The identified *ptpra*^{hu3334} allele has a TTG–TAG codon change resulting in a L133X premature stop in the extracellular region of RPTPα, likely rendering the protein non-functional and henceforward referred to as *ptpra+/−* for heterozygous and *ptpra−/−* for homozygous mutant alleles (Fig. 4A). Incrosses of heterozygous *ptpra+/−* fish led to morphological defects in a Mendelian ratio. These defects were detectable from 24 hpf onwards. In order to verify that RPTPα protein expression was affected, heterozygous *ptpra+/−* fish were incrossed and the offspring was sorted based on phenotype. At 52 hpf embryos were lysed and analyzed by immunoblotting with an anti-RPTPα antibody (Fig. 4B). RPTPα expression was readily detectable in morphologically wildtype embryos (siblings), whereas RPTPα protein was hardly detectable in mutant embryos. Expression of actin was monitored to control for equal protein loading. The genotype of the embryos that were used for immunoblotting could not be determined because lysis for immunoblotting is not compatible with genotyping procedures. Nevertheless, these results demonstrate that RPTPα protein expression is abolished in roughly a quarter of the offspring of an incross of heterozygous *ptpra+/−* fish, which are likely homozygous mutant embryos.

Incrosses of *ptpra+/−* fish were separated based on morphology and development was followed over time. Finally, the genotype of these embryos was determined by sequencing of ptpra exon 3. Homozygous mutant embryos can be identified as early as 24 hpf, having shorter yolk extensions and a shorter body axis (Figs. 4C, F, arrow). Starting from around 48 hpf these embryos developed cardiac edemas (Figs. 4D, G). The phenotype of *ptpra−/−* embryos was very similar to ptpra-MO injected embryos, as ptpra-MO injected embryos generally had shorter yolk extensions and also developed cardiac edemas (*cf.* Figs. 4D and 2B). At later stages these edemas grew bigger and caused blood circulation to stop. Homozygous mutant embryos died around 5–6 dpf with massive cardiac edemas.

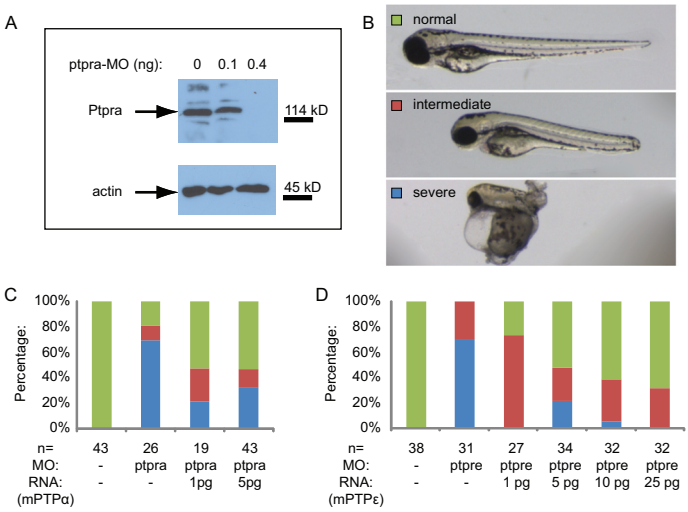

Fig. 3. RPTPα knockdown abolished protein expression and both RPTPα and PTPε knockdowns were rescued by co-injection of RNA.
(A) Zebrafish embryos were microinjected at the 1 cell stage with ptpra-MO (0.1 ng/embryo or 0.4 ng/embryo) and grown to 52 hpf. Embryos were dechorionated, deyolked and lysed using sodium orthovanadate and protease inhibitors. Samples of non-injected control and MO injected embryos were loaded on SDS-PAGE in such a way that all samples contain equal amounts of protein. Immunoblots were analyzed for expression of RPTPα and actin as a loading control. (B–D) Zebrafish embryos were micro-injected with ptpra-MO (C) or ptpre-MO (D) with or without mRNA encoding mouse RPTPα (C) or PTPε (D). Embryos were grown to 2 dpf and phenotypes were assigned as indicated in panel B, where embryos scored as normal resemble non-injected control, embryos with overall normal looking phenotype and body plan but shortened body axis were labeled as intermediate, and embryos with severely disrupted morphology were labeled severe.

The morphological defects from 24 hpf onwards were consistent with defects in C&E cell movements during gastrulation that are known to result in reduced embryonic axis extension. To verify that *ptpra−/−* mutants have defective C&E movements, embryos from *ptpra+/−* incrosses were fixed at the 1 somite stage and stained for *dlx3* and *hgg1* using whole mount *in situ* hybridization (Fig. 4I). The embryos were scored in a similar fashion as described above. After individual staining and scoring, the embryos were genotyped. Whereas the phenotype was not fully penetrant, homozygous *ptpra* mutants displayed a significant increase in posterior shift of the hatching gland and widening of the neural plate, which was consistent with the RPTPα knockdown phenotype. Although no differences between wildtype siblings and heterozygous embryos were observed at later stages, heterozygous embryos sometimes appeared to show an intermediate phenotype when looking at *dlx3*/*hgg1* staining at the 1 somite stage. This might be due to a dosage effect but because the effect was not consistently observed, we did not investigate this any further. To verify that the observed phenotype was indeed caused by lack of RPTPα we injected embryos from a *ptpra+/−* incross at the 1 cell stage with 10 pg *zf-ptpra* mRNA. Injection of RNA reduced the number of mutant embryos showing defective C&E as assessed by analyzing *dlx3* and *hgg1* expression to levels observed in siblings (Fig. 4I). We conclude that homozygous *ptpra−/−* embryos display C&E defects that were rescued by microinjection of *ptpra* RNA.

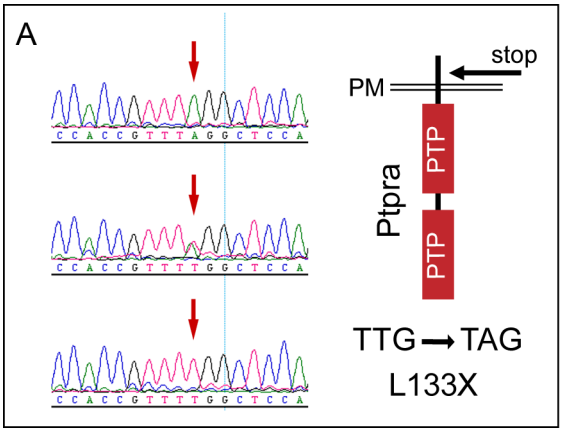
A
stop
PM
Ptpra
PTP
PTP
TTG → TAG
L133X

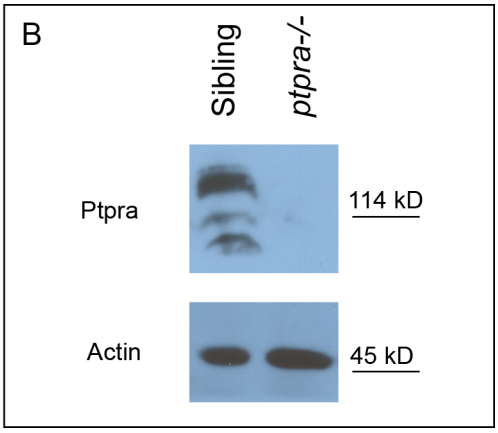
B
Sibling
ptpra-/-
Ptpra
114 kD
Actin
45 kD

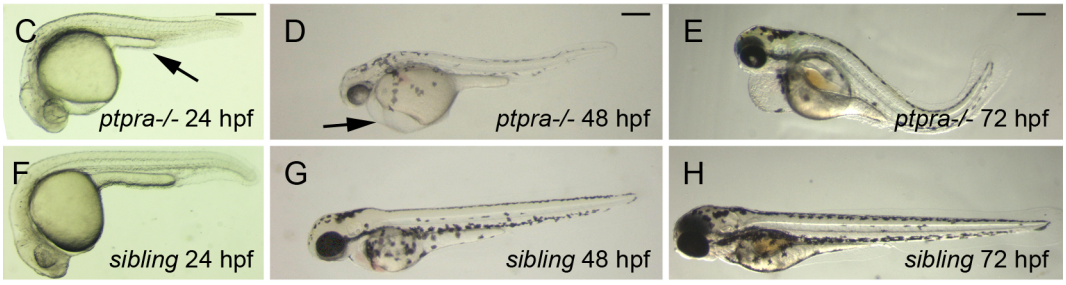
C
ptpra-/- 24 hpf
D
ptpra-/- 48 hpf
E
ptpra-/- 72 hpf
F
sibling 24 hpf
G
sibling 48 hpf
H
sibling 72 hpf

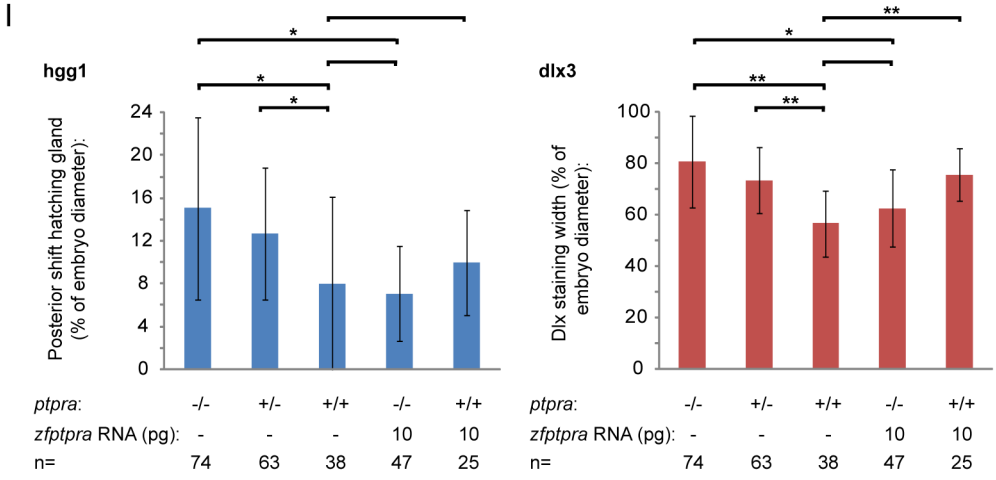
I
hgg1
Posterior shift hatching gland (% of embryo diameter):
24
20
16
12
8
4
0
ptpra: -/- +/- +/+ -/- +/+
zfptpra RNA (pg): - - - 10 10
n= 74 63 38 47 25
dlx3
Dlx staining width (% of embryo diameter):
100
80
60
40
20
0
ptpra: -/- +/- +/+ -/- +/+
zfptpra RNA (pg): - - - 10 10
n= 74 63 38 47 25

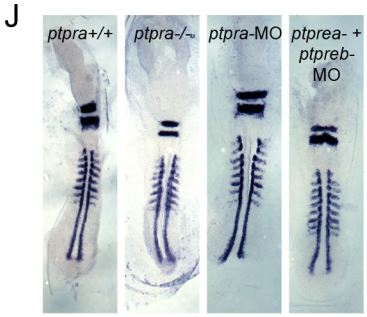
J
ptpra+/+
ptpra-/-
ptpra-MO
ptprea- + ptpreb-MO

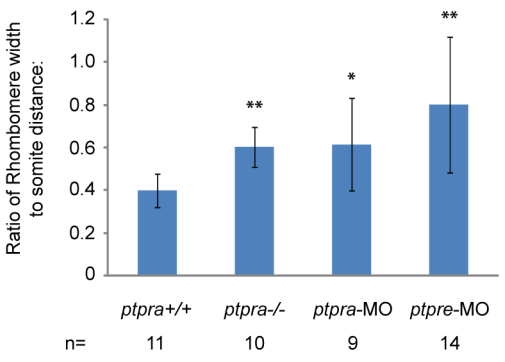
K
Ratio of Rhombomere width to somite distance:
1.2
1.0
0.8
0.6
0.4
0.2
0
ptpra+/+ ptpra-/- ptpra-MO ptpre-MO
n= 11 10 9 14

Fig. 4. A *ptpra* stop mutation phenocopied the ptpra knockdown and can be rescued by zf-ptpra mRNA.
(A) A *ptpra* mutant (hu3334) was identified by target selected gene inactivation. Homozygous mutant (top), heterozygous (middle) and wildtype (bottom) sequences are depicted here and the TTG to TAG codon change resulting in a L133X stop in the extracellular domain is indicated. (B) Heterozygous *ptpra+/−* fish were in-crossed and their offspring was grown to 52 hpf. Embryos were characterized as mutant or sibling based on observed phenotype, dechorionated, deyolked and lysed using sodium orthovanadate and protease inhibitors. The resulting lysates were analyzed for RPTPα expression. Actin expression was monitored as a loading control. Heterozygous *ptpra+/−* fish were in-crossed and offspring embryos were photographed and genotyped at 24 hpf (C, F), 48 hpf (D, G) and 72 hpf (E, H). Mutants (A–C) and siblings (D–F) are shown. (I) Heterozygous *ptpra+/−* fish were in-crossed and embryos were either grown to 1 somite stage and fixed without injection, or micro-injected at the one cell stage with 10 pg/embryo *zf-ptpra* mRNA and then grown to 1 somite stage and fixed. Whole mount *in situ* staining was performed using probes for *dlx3* and *hgg1*. The resulting staining patterns were analyzed by measuring the posterior shift of the hatching gland and the width of the *dlx3* staining as described in Fig. 2H. After pictures were taken embryos were lysed and genotyped. The average posterior shift of the hatching gland (*hgg1*) or width of the *dlx3* staining is plotted as a percentage of the embryo (yolk) diameter. (J) Heterozygous *ptpra+/−* fish were in-crossed and embryos were grown to 8 somite stage and fixed, or wildtype embryos were micro-injected at the one cell stage with 0.3 ng/embryo ptpra-MO or ptpre-MO and then grown to 8 somite stage and fixed.Whole mount in situ staining was performed using probes for *krox20* and *myod*. The resulting staining patterns were analyzed by measuring the rhombomere width and the distance from the 1st to the 8th somite. *Ptpra* incross embryos were subsequently genotyped. For each group a representative embryo is shown. The rhombomere width and the distance from the 1st to the 8th somite were measured. The resulting ratio was plotted (K). Mutant and knockdown embryos were compared to wildtype embryos. Error bars in all graphs indicate standard deviations, Student t-tests were performed (2 tailed, assuming unequal variance) between indicated groups where ** indicates a P-value<0.001, * a P-value<0.05 and no asterisk indicates no significant difference, P-value<0.05. Scalebars=250 μm.

To further characterize the C&E defect phenotype in mutant and knockdown embryos we performed *in situ* hybridization experiments with *krox20* and *myod* probes at the 8 somite stage (Li et al., 2008) (Fig. 4J). We analyzed mutant and knockdown embryos and compared them to wildtype siblings by determining the ratio of rhombomere width and distance from the 1st to the 8th somite (Fig. 4K). We found a significant increase in rhombomere width to somite distance ratio, indicating shorter and wider embryos. These results are consistent with the conclusion that the loss of RPTPα or PTPε by knockdown or mutation led to C&E defects.

RPTPα and PTPε do not affect cell specification

RPTPα and PTPε have been reported to affect several distinct signaling pathways (Gil-Henn and Elson, 2003; Lacasa et al., 2005; Maksumova et al., 2005; von Wichert et al., 2003). These pathways may affect cell specification, which may hamper interpretation of the results from the *dlx3*/*hgg1* staining, in that defects

in cell specification may be mistaken for C&E defects. To ensure that cell specification is not affected and the defects we observed in the experiments described above are due to C&E cell movements, we performed *in situ* hybridization with 6 hpf old MO injected embryos, mutant embryos and siblings using a panel of markers that are all known to be involved in cell specification (Fig. 5): *bone morphogenetic protein 2b* (*bmp2b*) specifies cells with ventral fates, *chordin* (*chd*) and *goosecoid* (*gsc*) are dorsalizing factors in the zebrafish organizer and *notail* (*ntla*) is a mesodermal marker. None of these markers displayed any major differences when RPTPα or PTPε knockdown or mutant embryos were compared to sibling embryos. *Goosecoid* expression in *ptpra−/−* embryos appeared to be located more towards the leading edge and was not properly localized towards the animal pole, which might reflect C&E cell migration defect. Taken together, these results show that dorsal–ventral specification was not affected in homozygous *ptpra* mutant, RPTPα or PTPε knockdown embryos, suggesting that the observed defects were due to defective morphogenetic cell movements, not to defects in cell specification during gastrulation.

Visualizing C&E cell migration patterns and intercalation

In order to visualize C&E cell movements, we proceeded to track epiblast cells during zebrafish gastrulation using confocal fluorescent microscopy. Zebrafish embryos were injected at the 1 cell stage with fluorescently labeled Histone 1 (H1) protein, labeling all nuclei. For time-lapse imaging the embryos were dechorionated at 30% epiboly and mounted at shield stage in 1% low melting point agarose. The H1-injected embryos were positioned with the dorsal side against the coverslip approximately 100 μm anterior to shield position and im-

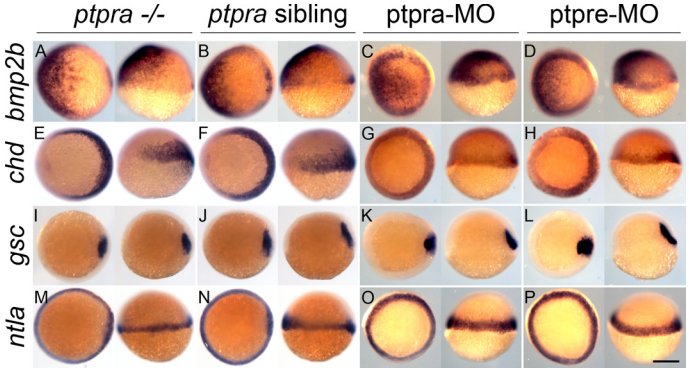

Fig. 5. No cell specification defects in *ptpra* mutant or RPTPα and PTPε knockdown embryos. Embryos were fixed at 6 hpf and whole mount in situ hybridization was performed using probes for *bmp2b*, *chordin* (*chd*), *gooscoid* (*gsc*) or *no tail* (*ntla*). Embryos from *ptpra+/−* incrosses were processed and genotyped after *in situ* hybridization. Alternatively, embryos injected at the 1-cell stage with ptpra-MO (0.3 ng/embryo) or ptpre-MO (2.5 ng ptprea-MO+2.5 ng ptpreb-MO/embryo) were used. Each panel depicts on the left: animal pole view with dorsal to the right; on the right: lateral view with dorsal to the right. Scale bar=250 μm.

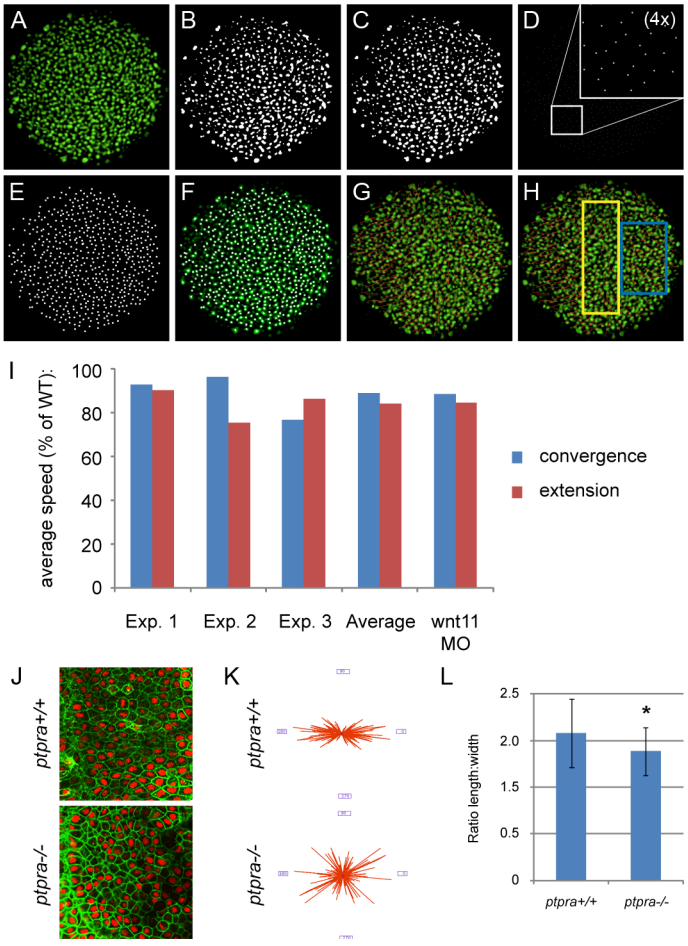

Fig. 6. Decreased convergence and extension cell migration speed and cell intercalation in ptpra−/− mutant.

Image processing used for cell tracking in order to quantify migration speeds: (A) original single Z-slice image acquired by confocal imaging of a wildtype embryo micro-injected with fluorescently labeled Histone 1 protein, (B) binary image, (C) binary image processed by watershedding, (D) all objects are eroded to a single pixel (inset shows 4× magnification for clarity), (E) every pixel is dilated, (F) projection of the resulting objects used for tracing onto the original image, (G) tracks generated by tracking algorithm projected onto the original image, (H) tracks generated by tracking algorithm projected onto the original image; the yellow rectangle indicates the area where tracks for extension speeds are collected, the blue rectangle represents the area where tracks for convergence speeds are collected. (I) *Ptpra+/−* fish were in-crossed and embryos were injected with Alexa Histone 1. Subsequently, 4–6 embryos were imaged in parallel using confocal microscopy starting from shield stage. Images were processed as described above and average cell migration speed was calculated by dividing the track length by the number of frames. For every experiment the average speed was calculated in either the convergence or the extension direction for typically more than 1000 cells per embryo. The embryos were subsequently genotyped and the average convergence and extension speeds in *ptpra−/−* mutant embryos were plotted as a percentage of the average speeds in wildtype siblings for every experiment individually. The average of the 3 experiments is indicated as well. As a positive control, convergence and extension speed was determined in *wnt11* knockdown embryos, that are well known to have convergence and extension cell movement defects. The average reduction determined in 3 independent experiments is shown. (J) *Ptpra+/−* fish were in-crossed and embryos were injected with YFP-CAAX and H2A-mCherry RNA. Embryos were mounted and imaged at late gastrulation stage posterior of the future site of the first somite in the region next to the notochord. After imaging embryos were genotyped. Shown are mutant and wildtype embryos. Obtained images were processed and the angles of cells were determined using ImageJ software and Shape_Descriptor1u plugin (Syverud et al., 2007). Resulting angles are from 2 mutant embryos and 2 wildtype embryos and are plotted in a rose diagram (K). Length and width of the cells were determined in a similar fashion and the ratios were plotted (L). Mutants were compared to wildtype data using Student t-test, error bars represent standard deviation, asterisk indicates a P-value<0.001.

aged at 40x magnification. At this position the C&E movements of the epiblast can be clearly visualized. We recorded from shield stage until 1-somite stage with 2 minute intervals. Time-lapse images were analyzed using ImageJ. The nuclear labeling was used to determine the position of individual cells in a single optical slice for each time point (Fig. 6A). To account for z-drift the imaged volume region included the enveloping layer (EVL), epiblast, hypoblast, and the yolk syncytial layer with 4 μm spacing between the z-positions. The difference between the epiblast and EVL was straightforward since the EVL nuclei were larger and clearly distinguishable from epiblast nuclei. The difference between hypoblast and epiblast was evident because of the difference in dynamics of the axial mesendoderm cells to the overlaying epiblast. From shield stage to 65%–70% epiboly the axial mesendoderm cells migrated anteriorly while the overlying epiblast cells were slightly moving towards the vegetal pole undergoing the early gastrulation epiboly movement. The layers were also clearly separated by Brachet's cleft. Using these parameters the z-position of the epiblast cells was readily determined in the data. 2D cell tracing for the epiblast was performed at this z-position. In case of z-drift the position of tracing was adjusted accordingly to a lower or higher position at the time point of the drift.

Cell tracing, C&E analysis and image processing

Time-lapse images were analyzed using ImageJ. This 2D image analysis program was amenable at this magnification in this region because the imaged region used for analysis was approximately flat and the region got even more flattened because of the positioning against the coverslip. The slight tissue curvature which was still apparent was both present in the mutant and wt control embryos and as such accounted for when calculating the relative differences of the cell migrations (data not shown). In the images the embryo was positioned with the anterior side towards the top of the image. The Cartesian coordinates of cell tracks generated in this way represented the contribution of cell migration to convergence (X-axis) and extension (Y-axis). The cells were readily traced after some image processing (see below) with an algorithm that implemented feature point detection and tracking (Sbalzarini and Koumoutsakos, 2005). The algorithm generated a report with the Cartesian coordinates for all traced objects at each time point. Using the coordinates we were able to calculate >1000 cell movements per analyzed embryo, which were used to determine the average contribution of the individual cell tracks to convergence (Y-direction) or extension (X-direction, Fig. 6H). Tracks used for the analysis of extension were calculated from cells at the axial epiblast region at time points between 70% and 90% epiboly. Tracks used for the analysis of convergence were calculated from cells at the paraxial region at time points between 90% epiboly and 1-somite stage from the same dataset.

Due to the innate changes in intensity, size and shape of H1 signal of the

nuclei, we developed additional image processing for efficient tracing of the cells. Making the images binary solves the problem of variable fluorescent intensities (Fig. 6B). The occasional occurrence of fused objects was handled by a water-shedding process which reseparated most fused objects (Fig. 6C). These objects still changed during the time-lapse run in size and shape. Eroding every object to a single pixel generated an image with single point markings representing the individual positions of each object (Fig. 6D). For tracing purposes these single pixels were dilated (Fig. 6E). When the resulting image was re-projected onto the original it was evident that the generated objects represented cell positions with a very high accuracy (>99%, Fig. 6F).

Reduced C&E movements in ptpra−/− embryos

We used the tracking method described above to quantify C&E cell movements in *ptpra−/−* embryos and to compare with wildtype siblings. To this end, heterozygous *ptpra+/−* fish were in-crossed and four to six embryos were mounted and imaged as described above. When comparing *ptpra−/−* mutants with wildtype embryos great precaution was taken to position the embryos in a similar way. The exact imaging position was determined retrospectively using embryonic features, including otoliths and somites that had developed at the end of the run as coordinates. Data from embryos that were not positioned correctly or that moved slightly during imaging were discarded. Following imaging, the embryos were genotyped by sequencing. The relative speed of cells in *ptpra−/−* embryos compared to wildtype siblings from 3 independent experiments is plotted in Fig. 6I. We consistently found a reduction in migration speed in both X-direction (convergence) and Y-direction (extension) for mutant embryos. The statistical analysis has been performed by Student t-test assuming unequal variances with alpha=0.05. Since the data for every experiment consisted of over 1000 datapoints for every experiment, *P*-values were much lower than 0.0001. We still detected a fluctuation between values of the relative speed for mutants between experiments, which could be accounted for by small differences from experiment to experiment in temperature inside the imaging chamber or slight differences in positioning of the embryo. In order to validate our method we used a well known regulator of C&E to assess its effect on cell migration speed in our setup. We used wnt11-MO injected embryos and found a reduction in migration speed compared to non-injected siblings in convergence (12%) and extension (15%), which was comparable to the measured reduction of migration speed in *ptpra−/−* embryos compared to siblings (Fig. 6I). In conclusion, we have developed a method to reliably quantify C&E cell movements using time-lapse confocal microscopy. Using this method, we found that the average relative speed of C&E cell movements during gastrulation was significantly reduced in *ptpra−/−* mutant embryos compared to wildtype siblings.

Mutant embryos have cell intercalation defects

One of the underlying mechanisms of C&E is cell intercalation and mediolateral elongation (Concha and Adams, 1998; Myers et al., 2002). We used membrane labeling by YFP-CAAX to determine the cell shape of intercalating cells in late gastrulation. Injected embryos were mounted and the presomitic mesoderm was imaged posterior to the site of the future first somite in the region neighboring the notochord as described (Jessen et al., 2002). We used ImageJ software and the Shape_Descriptor1u plugin (Syverud et al., 2007) to analyze the angle of the cells towards the notochord and the ratio of length to width of the cells. We found that indeed in *ptpra−/−* mutants the ratio of length:width is significantly reduced (Student t-test, $P<0.001$) and angles towards the notochord are distributed more randomly (Figs. 6J–L). This further reinforces the role of RPTPα in C&E.

Simultaneous knockdown of RPTPα and PTPε phenocopied silberblick

C&E movements are regulated by the non-canonical Wnt signaling pathway. The main players in this pathway are Wnt5 and Wnt11, which activate downstream Rho-like GTPases instead of β-catenin as is the case in canonical Wnt signaling (Veeman et al., 2003). Mutation or knockdown of Wnt11 results in defects in embryonic axis extension in the anterior regions of the embryo (Heisenberg et al., 2000), whereas mutation or knockdown of *wnt5* results in defects in the posterior regions of the embryo (Kilian et al., 2003), reflecting the expression patterns of Wnt11 and Wnt5, respectively. As shown above, co-injection of ptpra-MO and ptpre-MO caused a phenotype resembling the *wnt11* mutant/*silberblick* phenotype. Co-injection of ptpra-MO and ptpre-MO resulted in severe defects and early embryonic lethality. At lower concentrations, co-injection resulted in cyclopia in ~10% of the embryos (data not shown). Injection of ptpre-MO in *ptpra−/−* fish resulted in cyclopic fish as well (data not shown). We proceeded to quantify the number of cyclopic fish upon co-injection of ptpra-MO and ptpre-MO with Wnt11-MO (Fig. 7). Low amounts of ptpre-MO together with low concentrations of Wnt11-MO induced a high percentage of cyclopic fish (>60%), whereas ptpra-MO together with Wnt11-MO induced a high percentage of fish with a severe phenotype (>60%). Injection of single morpholinos at these reduced concentrations resulted in hardly any phenotype (Fig. 7). Together, these results suggest that RPTPα and PTPε function either in the same pathway as Wnt11, or they have a common downstream target with Wnt11.

RPTPα and PTPε signal upstream of RhoA and Fyn/Yes

The major downstream targets of the non-canonical Wnt signaling pathway are the small GTPases, Rac and RhoA. To test if these might be common downstream targets for both Wnt11 signaling and RPTPα and PTPε, we investigated whether co-injection of mRNA coding for constitutively active Rac or RhoA res-

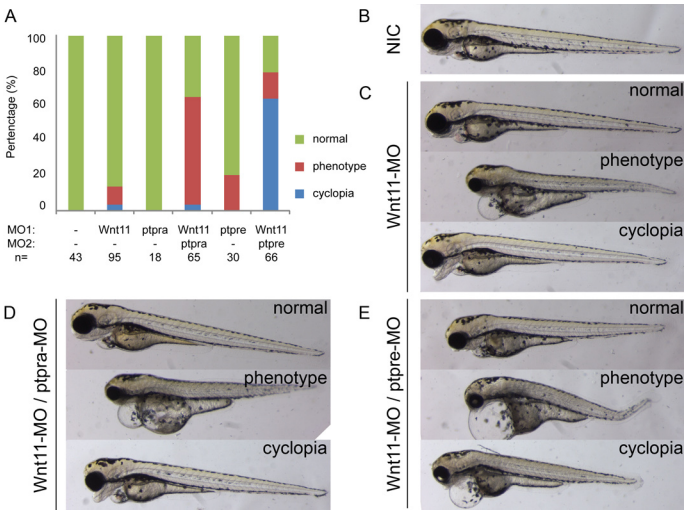

Fig. 7. RPTPα and PTPε knockdown phenotypes were enhanced by *wnt11* knockdown and induced cyclopia.
(A) Zebrafish embryos were injected with low amounts of morpholino targeting RPTPα (0.15 ng/embryo), PTPε (1 ng each/embryo) and Wnt11 (2 ng/embryo) and grown to 3 dpf. Embryos were scored based on morphology "cyclopia" when eyes were fused, as "phenotype" when shorter, showing abnormal morphology and/or edemas, or as "normal". The percentages of embryos with phenotypes were plotted. Representative embryos from each (co-)injection are depicted in panels B–E.

cued the observed C&E phenotypes. We found that both caRac and caRhoA mRNA produced severe phenotypes when injected at high doses (data not shown), and titrated to find concentration ranges that might be suitable for rescue experiments.We found that injection of 2 pg caRhoA RNA per embryo or less did not induce any phenotypes by itself. Injection of 0.5 pg caRac RNA per embryo still induced truncated or shorter embryos. We co-injected ptpra-MO or ptpre-MO with either 1 pg caRhoA RNA or 0.5 pg caRac RNA and found that the penetrance and severity of the phenotype was reduced by co-injection of caRho RNA, but not caRac RNA (Figs. 8A, B). As read-out for the phenotype we measured body axis extension, i.e. the length of the tail, a hallmark of C&E defects (as indicated in Fig. 8B). Co-injection of caRhoA RNA led to a significant increase in body length compared to ptpra-MO or ptpre-MO alone, but caRac RNA did not alleviate the body axis extension defect (Fig. 8B). These results indicate that caRhoA, but not caRac, rescued the RPTPα and PTPε knockdown phenotypes.

CaRac or caRhoA RNA was injected in *ptpra+/–* incross embryos and C&E defects were determined by *dlx3/hgg1* whole mount in situ hybridization at the 1 somite stage. It is noteworthy that the phenotypes were assigned and afterwards, embryos were genotyped. We found that caRhoA significantly rescued C&E defects in *ptpra–/–* embryos (Fig. 8C). CaRac improved the extension phenotype slightly as assessed by *hgg1* staining, but convergence, measured by *dlx3* staining was not rescued significantly. We generally observed that injection of caRac RNA induced poor overall morphology in mutant as well as wildtype embryos at later stages and hence we cannot conclude that caRac rescued the *ptpra–/–* pheno-

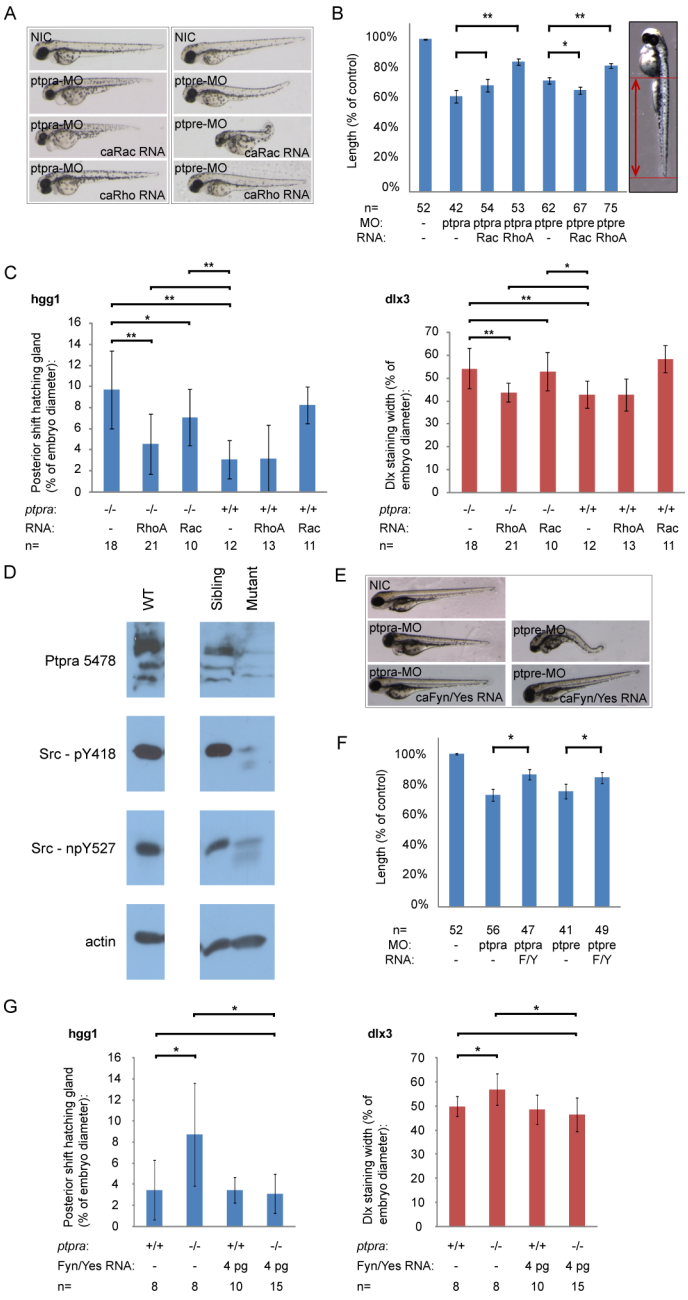

Fig. 8. RPTPα and PTPε knockdown rescued by active RhoA or active Fyn and Yes.

(A) Zebrafish embryos were microinjected at the 1-cell stage with ptpra-MO (0.3 ng/embryo) or ptpre-MO (2.5 ng ptprea-MO+2.5 ng ptpreb-MO/embryo) alone or co-injected with active Rac (1 pg/embryo) or RhoA (1 pg/embryo) mRNA. Embryos were grown to 2 dpf. Morpholino knockdown and RNA co-injection rescue experiments were done in the same clutch of embryos. The figure depicts representative embryos for every group from two independent experiments. (B) The phenotypes of all individual fish depicted in (A) were assessed by measuring tail lengths using ImageJ software. Tail lengths were depicted as a percentage of the length of non-injected control embryos. The figure represents the results of two independent experiments, where morpholino knockdown and RNA co-injection rescue experiments were performed in the same clutches of embryos. RNA co-injections were compared to their respective morpholino injections and Student t-tests were applied.* represents a P-value<0.05, ** represents a P-value<0.001, no asterisk represents no significant difference (P>0.05). (C) Heterozygous *ptpra+/–* fish were in-crossed and offspring embryos were micro-injected at the 1-cell stage with either active Rac or active RhoA mRNA. Non-injected embryos were taken as a control. Embryos were grown to 1 somite stage and fixed. Whole mount *in situ* staining was performed using probes for *dlx3* and *hgg1*. The resulting staining patterns were analyzed as described in Fig. 2H, by measuring the posterior shift of the hatching gland and the width of the *dlx3* staining. After pictures were taken and phenotypes were assigned, embryos were lysed and genotyped. The average posterior shift or width of the *dlx3* is plotted as a percentage of the embryo (yolk) diameter. (D) Heterozygous *ptpra+/–* or wildtype (WT) fish were in-crossed and their offspring was grown to 52 hpf. Embryos were characterized as mutant or sibling based on observed phenotype, dechorionated, deyolked and lysed using sodium orthovanadate and protease inhibitors. Western blots were run and probed using 5478-anti RPTPα serum, Src-pY418 antibody, Src-npY527 antibody and actin

antibody as a loading control. (E) Embryos were injected with ptpra-MO (0.3 ng/embryo) or ptpre-MO (2.5 ng ptprea-MO+2.5 ng ptpreb-MO/embryo) like in figure (A) and co-injections were done with active Fyn and Yes (4 pg each/embryo) RNA. Figure represents two separate experiments; morpholino injection and RNA co-injections were done in the same clutches of embryos. A representative embryo for each injected group is shown. (F) The lengths of the embryos' tails were measured and the average was plotted. (G) Heterozygous *ptpra+/–* fish were in-crossed and embryos were micro-injected in a similar fashion as in (C) with 4 pg/embryo of both active Fyn and Yes mRNA. The embryos were stained for *dlx3* and *hgg1*, analyzed and genotyped and the posterior shift of the hatching gland and the width of the *dlx3* staining were plotted for each group. Error bars in all graphs represent standard deviations. Student t-tests were performed between indicated groups, where ** indicates a P-value<0.001, * a P-value<0.05 and no asterisk no significant difference (P-value>0.05).

type. Our results indicate that caRhoA rescued the *ptpra–/–* induced C&E defects, consistent with the caRhoA rescue of the ptpra-MO knockdown.

We recently described how Fyn and Yes play a role in C&E in zebrafish by activating RhoA in parallel with the non-canonical Wnt signaling pathway (Jopling and den Hertog, 2005). RPTPα dephosphorylates the inhibitory tyrosine phosphorylation site in the C-terminus of Src family kinases (Tyr 527 in chicken Src) thus resulting in activation of the Src family kinases (den Hertog et al., 1993; Zheng et al., 1992). Therefore we wondered whether Src family kinase phosphorylation was affected in *ptpra–/–* zebrafish embryos. At 24 hpf, embryos from a *ptpra+/–* incross were divided in two groups based on morphology: mutants and siblings. The embryos were lysed at 52 hpf and lysates were immunoblotted. As a control, RPTPα expression was monitored in these lysates (Fig. 8D). RPTPα protein was not detected in the mutants. The Src nonphospho (np)Tyr527 antibody is specific for non-phosphorylated Tyr527. The signal is clearly reduced in *ptpra–/–* mutants, indicating that phosphorylation of this site is enhanced in mutant embryos that do not express RPTPα. Phosphorylation of Tyr416, the autophosphorylation site of Src family kinases is directly proportional to its activation state. Tyr416 phosphorylation is reduced dramatically in mutants, reflecting reduced activity of Src family kinases as a result of enhanced phosphorylation of the inhibitory Tyr527. These results demonstrate that phosphorylation of the inhibitory C-terminal Tyr527 in Src is enhanced resulting in reduced Src activity which is reflected by reduced autophosphorylation of Tyr416.

To investigate directly whether the observed defects upon knockdown of RPTPα and PTPε were linked to Src family kinases, we co-injected RNA encoding active Fyn and Yes with ptpra-MO or ptpre-MO and assessed body axis extension. It is evident that Fyn and Yes significantly rescued both RPTPα knockdown as well as PTPε knockdown (Figs. 8E, F). Moreover when we injected active Fyn and Yes mRNA in *ptpra+/–* incross embryos and assessed the phenotype in a similar fashion as in Fig. 8C, we observed a clear reduction of the posterior shift of the

hatching gland and reduction of the width of *dlx3* staining in mutant embryos to the level of wildtype sibling (Fig. 8G), indicating that activation of the SFKs Fyn and Yes rescued the *ptpra−/−* induced C&E phenotype. Our results demonstrate that Src family kinase activity was reduced in *ptpra−/−* fish and that Src family kinases rescued RPTPα and PTPε knockdown induced defects, firmly placing Src family kinases downstream of RPTPα and PTPε in C&E cell movements.

Discussion

C&E cell movements during gastrulation are tightly regulated by several signaling pathways, including non-canonical Wnt signaling and signaling by Src family kinases. Here, we provide evidence that RPTPα and PTPε are essential for C&E cell movements during gastrulation as well. RPTPα and PTPε knockdown embryos as well as *ptpra−/−* embryos displayed C&E defects, which were rescued by co-injection of synthetic RNAs encoding the respective proteins. We developed a cell tracking method using confocal time-lapse microscopy, which allowed us to quantify cell movements of all cells in the developing embryo. We have used this method to demonstrate that both convergence and extension cell movements were reduced in *ptpra−/−* embryos. RPTPα and PTPε signal upstream of Src family kinases and the small GTPase RhoA to regulate C&E cell movements.

RPTPα and PTPε function in C&E movements

During axis formation in vertebrate gastrulation, dorsal mesendodermal cells become highly motile and polarized, a process regulated in part by rearrangements of actin cytoskeleton. These cells move to the midline where they intercalate, which results in extension of the embryonic body axis. We demonstrate here that RPTPα and PTPε are involved in these processes and we propose that the underlying mechanism involves controlling the activity of downstream targets of the non-canonical Wnt signaling pathway. Whether the C&E defects result from reduced polarization of the cells, reduced cell adhesion or an impaired chemotactic response remains to be determined. However, these data do not simply reflect a delay in development since mutant embryos reached the 1 somite stage at the same time as sibling or wildtype embryos (data not shown). Cell specification was not affected in RPTPα or PTPε knockdown embryos or *ptpra−/−* embryos, ruling out that defective cell specification was at the basis of the observed defects.

Cell tracking

We adapted and employed a method to efficiently track cells in the developing embryo using time-lapse confocal microscopy. Recently, *in toto* imaging was described for zebrafish embryos in which all cells were visualized and tracked over a period of 24 h (Keller et al., 2008). Scanned light sheet microscopy was employed to allow for rapid scanning through the entire embryo. We were

interested particularly in C&E cell movements during gastrulation and we used conventional time-lapse confocal microscopy to image cell movements in an area anterior to the shield, where C&E cell movements take place during gastrulation. We improved ImageJ software, allowing us to automatically track large numbers of cells in the area of interest and to quantify cell movements in this area. Whereas we imaged the cells in 3D, we employed the data analysis in 2D, because the distortion resulting from the curvature of the embryo was minimal (up to 6% at the edges of the image, data not shown). Using this method, we reliably calculated the velocities of many individual cells and we compared C&E movements of more than 1000 cells in three independent *ptpra−/−* embryos with those of cells in wildtype siblings in three independent experiments. We detected significant differences in cell movements in all three experiments with on average 11% reduced convergence and 16% reduced extension (Fig. 6). In principle this method can be used to detect changes in all kinds of cell movements and only requires time-lapse imaging using a conventional (confocal) microscope.

Signaling driving C&E cell movements

The β-Catenin independent wnt-PCP signaling pathway has been shown to control C&E movements (Wallingford et al., 2002). Key events in the regulation of C&E movements are the activation of RhoA and Rac1 (Habas et al., 2001; Tahinci and Symes, 2003). We have identified several other proteins that modulate this pathway, including Shp2, Csk, Fyn and Yes (Jopling and den Hertog, 2005; Jopling and den Hertog, 2007; Jopling et al., 2007). Moreover, Has2, PAPC and STAT3 have a role in the pathway as well (Bakkers et al., 2004; Miyagi et al., 2004; Unterseher et al., 2004). All of these proteins act in C&E movements by changing the activity of RhoA and/or Rac1 in dorsally migrating cells during gastrulation.

Several lines of evidence suggest a role for RPTPα and PTPε in non-canonical Wnt signaling. Co-injection of ptpra-MO and ptpre-MO or injection of ptpre-MO in *ptpra−/−* embryos resulted in cyclopia (Fig. 7), a phenotype also observed in *wnt11* mutant fish (Heisenberg et al., 1996). Co-injection of low amounts of Wnt11-MO together with low amounts of ptpra-MO or ptpre-MO specifically caused cyclopia and severe phenotypes in fish, suggesting that Wnt11 and RPTPα and PTPε interact genetically. We attempted to rescue the Wnt11 knockdown phenotype by co-injection of *ptpra* or *ptpre* RNA. Coinjection of these synthetic RNAs at concentrations that rescued the respective ptpra- and ptpre-MO injections (Fig. 3) did not rescue the Wnt11-MO phenotype in a significant way (data not shown). This is consistent with our previous finding that the Src family kinases, Fyn and Yes, act in a signaling pathway parallel to non-canonical Wnt signaling, converging on RhoA. RPTPα and PTPε have been shown to dephosphorylate and activate Src family kinases in cell-based assays. Here, we demonstrate that Src family kinase phosphorylation on the inhibitory C-terminal residue (Tyr527)

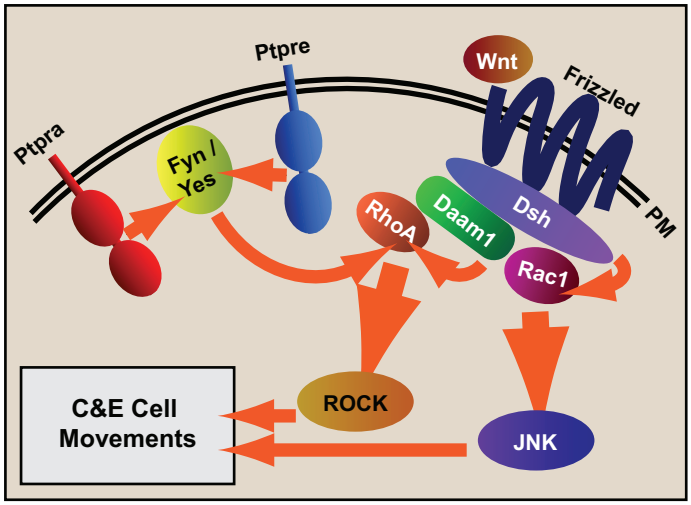

Fig. 9. RPTPα and PTPε act in parallel to non-canonical Wnt signaling in C&E cell movements. In non-canonical Wnt signaling, Frizzled is activated by binding of Wnt which results in Dishevelled (Dsh) and Daam1-mediated activation of RhoA and Rac1. In turn, Rac1 and RhoA activate Jun N-terminal Kinase (JNK) and ROCK, respectively, leading to cell polarization, actin cytoskeleton rearrangements and cell movements. RPTPα and PTPε dephosphorylate and activate the Src family kinases, Fyn and Yes, leading to downstream activation of RhoA through an unknown intermediate, thereby mediating convergence and extension cell movements.

was enhanced in *ptpra−/−* zebrafish embryos. Autophosphorylation (on Tyr416) was reduced, indicating that Src family kinase activity was reduced in zebrafish embryos lacking functional RPTPα. Interestingly, mutant *ptpra−/−* embryos and RPTPα and PTPε knockdowns were rescued by active Fyn and Yes, demonstrating that these Src family kinases indeed acted downstream of RPTPα and PTPε in the control of C&E cell movements (Fig. 8). Finally, we demonstrated that active RhoA, but not Rac1, rescued the RPTPα and PTPε knockdown and *ptpra−/−* mutant phenotype, similar to RhoA-mediated rescue of Wnt11 and Fyn/Yes knockdown (Jopling and den Hertog, 2005). These results led us to propose a model where RPTPα and PTPε act in C&E cell movements in a SFK dependent pathway parallel to non-canonical Wnt signaling, modulating downstream RhoA activity (Fig. 9).

RPTPα and PTPε knock out mice

Interestingly, RPTPα and PTPε and even RPTPα/PTPε double knock out (DKO) mice are viable (Tiran et al., 2006), whereas *ptpra−/−* zebrafish were embryonic lethal. Co-injection of ptpra-MO or ptpre-MO, resulting in transient knockdown of RPTPα or PTPε already caused lethality. DKO mice are shorter but retain a normal growth rate, which is consistent with a mild C&E defect phenotype. Detailed analysis of gastrulation in RPTPα and PTPε knock out mice may lead to identification of subtle or transient defects in gastrulation in these mice. Moreover, analysis of the orientation of stereociliary bundles in cochleae is one of the best read-outs for planar polarity in the mouse and several knock outs of factors from the non-canonical Wnt signaling pathway display defective bundle orientation (Montcouquiol et al., 2003). It will be interesting to analyze stereocili-

ary bundle orientation in RPTPα and PTPε knock out mice to establish whether these mice display subtle defects resembling the PCP signaling defects. It remains to be determined why there is a difference between mice and fish. Perhaps C&E movements are more easily affected by changes in activity of RPTPα and PTPε in zebrafish embryos, or perhaps zebrafish embryos lack factors that compensate for the absence of RPTPα and PTPε in mouse embryos. It will be interesting to see if DKO mice are shorter because of defects in Src family kinase signaling and/or RhoA activity. It is noteworthy that cell movements of pyramidal neurons in RPTPα knock out mice are defective (Petrone et al., 2003), and it will be interesting to see if defective RhoA signaling is at the basis of these cell movement defects in a similar manner as in C&E cell movements in zebrafish embryos.

Conclusion

In conclusion, we demonstrate here that RPTPα and PTPε have an essential role in C&E cell movements during gastrulation. Moreover, RPTPα and PTPε act in a signaling pathway upstream of Src family kinases and the small GTPase RhoA. It will be interesting to see what is upstream of RPTPα and PTPε. Our results demonstrate that the RPTP-SFK-RhoA signaling pathway is an important regulator of C&E cell movements next to the well known non-canonicalWnt/PCP signaling pathway.

Acknowledgments

This work was supported in part by a Marie Curie Research Training Network (PTPNET/MRTN-CT-2006-035830) and a grant from the Research Council for Earth and Life Sciences (ALW 815.02.007) with financial aid from the Netherlands Organisation for Scientific Research (NWO).

References

Ardini, E., Agresti, R., Tagliabue, E., Greco, M., Aiello, P., Yang, L.T., Menard, S., Sap, J., 2000. Expression of protein tyrosine phosphatase alpha (RPTPalpha) in human breast cancer correlates with low tumor grade, and inhibits tumor cell growth in vitro and in vivo. Oncogene 19, 4979–4987.

Bakkers, J., Kramer, C., Pothof, J., Quaedvlieg, N.E., Spaink, H.P., Hammerschmidt, M., 2004. Has2 is required upstream of Rac1 to govern dorsal migration of lateral cells during zebrafish gastrulation. Development 131, 525–537.

Chiusaroli, R., Knobler, H., Luxenburg, C., Sanjay, A., Granot-Attas, S., Tiran, Z.,Miyazaki, T.,Harmelin, A., Baron, R., Elson, A., 2004. Tyrosine phosphatase epsilon is a positive regulator of osteoclast function in vitro and in vivo. Mol. Biol. Cell 15, 234–244.

Concha, M.L., Adams, R.J., 1998. Oriented cell divisions and cellular morphogenesis in the zebrafish gastrula and neurula: a time-lapse analysis. Development 125, 983–994.

Courtneidge, S.A., 1985. Activation of the pp 60c-src kinase by middle T antigen binding or by dephosphorylation. EMBO J. 4, 1471–1477.

den Hertog, J., Hunter, T., 1996. Tight association of GRB2 with receptor proteintyrosine phosphatase alpha is mediated by the SH2 and C-terminal SH3 domains. EMBO J. 15, 3016–3027.

den Hertog, J., Pals, C.E., Peppelenbosch, M.P., Tertoolen, L.G., de Laat, S.W., Kruijer, W., 1993. Receptor protein tyrosine phosphatase alpha activates pp 60c-src and is involved in neuronal differentiation. EMBO J. 12, 3789–3798.

den Hertog, J., Tracy, S., Hunter, T., 1994. Phosphorylation of receptor protein-tyrosine phosphatase alpha on Tyr789, a binding site for the SH3–SH2–SH3 adaptor protein GRB-2 in vivo. EMBO J. 13, 3020–3032.

Gil-Henn, H., Elson, A., 2003. Tyrosine phosphatase-epsilon activates Src and supports the transformed phenotype of Neu-induced mammary tumor cells. J. Biol. Chem. 278, 15579–15586.

Goldstein, B., Takeshita, H., Mizumoto, K., Sawa, H., 2006. Wnt signals can function as positional cues in establishing cell polarity. Dev. Cell 10, 391–

396.

Griffin, K., Patient, R., Holder, N., 1995. Analysis of FGF function in normal and no tail zebrafish embryos reveals separate mechanisms for formation of the trunk and the tail. Development 121, 2983–2994.

Habas, R., Kato, Y., He, X., 2001. Wnt/Frizzled activation of Rho regulates vertebrate gastrulation and requires a novel Formin homology protein Daam1. Cell 107, 843–854.

Habas, R., Dawid, I.B., He, X., 2003. Coactivation of Rac and Rho by Wnt/Frizzledsignaling is required for vertebrate gastrulation. Genes Dev. 17, 295–309.

Hannus, M., Feiguin, F., Heisenberg, C.P., Eaton, S., 2002. Planar cell polarization requires Widerborst, a B′ regulatory subunit of protein phosphatase 2A. Development 129, 3493–3503.

Heisenberg, C.P., Brand, M., Jiang, Y.J., Warga, R.M., Beuchle, D., van Eeden, F.J., Furutani-Seiki, M., Granato, M., Haffter, P., Hammerschmidt, M., Kane, D.A., Kelsh, R.N.,

Mullins, M.C., Odenthal, J., Nusslein-Volhard, C., 1996. Genes involved in forebrain development in the zebrafish, Danio rerio. Development 123, 191–203.

Heisenberg, C.P., Tada, M., Rauch, G.J., Saude, L., Concha, M.L., Geisler, R., Stemple, D.L., Smith, J.C., Wilson, S.W., 2000. Silberblick/Wnt11 mediates convergent extension movements during zebrafish gastrulation. Nature 405, 76–81.

Herrera Abreu, M.T., Penton, P.C., Kwok, V., Vachon, E., Shalloway, D., Vidali, L., Lee, W., McCulloch, C.A., Downey, G.P., 2008. Tyrosine phosphatase PTPalpha regulates focal adhesion remodeling through Rac1 activation. Am. J. Physiol. Cell Physiol. 294, C931–C944.

Hsia, D.A., Lim, S.T., Bernard-Trifilo, J.A., Mitra, S.K., Tanaka, S., denHertog, J., Streblow,D.N., Ilic, D., Ginsberg, M.H., Schlaepfer, D.D., 2005. Integrin alpha4-beta1 promotes focal adhesion kinase-independent cell motility via alpha4 cytoplasmic domain-specific activation of c-Src. Mol. Cell. Biol. 25, 9700–9712.

Jessen, J.R., Topczewski, J., Bingham, S., Sepich, D.S., Marlow, F., Chandrasekhar, A.,Solnica-Krezel, L., 2002. Zebrafish trilobite identifies new roles for Strabismus in

gastrulation and neuronal movements. Nat. Cell Biol. 4, 610–615.

Jopling, C., den Hertog, J., 2005. Fyn/Yes and non-canonical Wnt signalling converge on

RhoA in vertebrate gastrulation cell movements. EMBO Rep. 6, 426–431.

Jopling, C., den Hertog, J., 2007. Essential role for Csk upstream of Fyn and Yes in

zebrafish gastrulation. Mech. Dev. 124, 129–136.

Jopling, C., van Geemen, D., den Hertog, J., 2007. Shp2 knockdown and Noonan/

LEOPARD mutant Shp2-induced gastrulation defects. PLoS Genet. 3, e225.

Keller, R., Shih, J., Domingo, C., 1992. The patterning and functioning of protrusive activity

during convergence and extension of the Xenopus organiser. Dev. Suppl. 81–91.

Keller, P.J., Schmidt, A.D.,Wittbrodt, J., Stelzer, E.H., 2008. Reconstruction of zebrafish early

embryonic development by scanned light sheetmicroscopy. Science 322, 1065–1069.

Kilian, B., Mansukoski, H., Barbosa, F.C., Ulrich, F., Tada, M., Heisenberg, C.P., 2003. The

role of Ppt/Wnt5 in regulating cell shape and movement during zebrafish

gastrulation. Mech. Dev. 120, 467–476.

Lacasa, D., Boute, N., Issad, T., 2005. Interaction of the insulin receptor with the

receptor-like protein tyrosine phosphatases PTPalpha and PTPepsilon in living

cells. Mol. Pharmacol. 67, 1206–1213.

Lele, Z., Bakkers, J., Hammerschmidt, M., 2001. Morpholino phenocopies of the swirl,

snailhouse, somitabun,minifin, silberblick, and pipetailmutations. Genesis

30, 190–194.

Li, C., Inglis, P.N., Leitch, C.C., Efimenko, E., Zaghloul, N.A., Mok, C.A., Davis, E.E., Bialas,N.J., Healy, M.P., Heon, E., Zhen, M., Swoboda, P., Katsanis, N., Leroux,M.R., 2008. An essential role for DYF-11/MIP-T3 in assembling functional intraflagellar transport complexes. PLoS Genet 4, e1000044.

Link, V., Shevchenko, A., Heisenberg, C.P., 2006. Proteomics of early zebrafish embryos. BMC Dev. Biol. 6, 1.

Maksumova, L., Le, H.T., Muratkhodjaev, F., Davidson, D., Veillette, A., Pallen, C.J., 2005. Protein tyrosine phosphatase alpha regulates Fyn activity and Cbp/PAG phosphorylation in thymocyte lipid rafts. J. Immunol. 175, 7947–7956

Matsui, T., Raya, A., Kawakami, Y., Callol-Massot, C., Capdevila, J., Rodriguez-Esteban, C., Izpisua Belmonte, J.C., 2005. Noncanonical Wnt signaling regulates midline convergence of organ primordia during zebrafish development. Genes Dev. 19,164–175.

Medina, A., Reintsch, W., Steinbeisser, H., 2000. Xenopus frizzled 7 can act in canonical and non-canonical Wnt signaling pathways: implications on early patterning and morphogenesis. Mech. Dev. 92, 227–237.

Myers, D.C., Sepich, D.S., Solnica-Krezel, L., 2002. Bmp activity gradient regulates convergent extension during zebrafish gastrulation. Dev. Biol. 243, 81–98.

Miyagi, C., Yamashita, S., Ohba, Y., Yoshizaki, H., Matsuda, M., Hirano, T., 2004. STAT3 noncell-autonomously controls planar cell polarity during zebrafish convergence and extension. J. Cell Biol. 166, 975–981.

Montcouquiol, M., Rachel, R.A., Lanford, P.J., Copeland, N.G., Jenkins, N.A., Kelley, M.W., 2003. Identification of Vangl2 and Scrb1 as planar polarity genes in mammals. Nature 423, 173–177.

Peretz, A., Gil-Henn, H., Sobko, A., Shinder, V., Attali, B., Elson, A., 2000. Hypomyelination and increased activity of voltage-gated K(+) channels in mice lacking protein tyrosine phosphatase epsilon. EMBO J. 19, 4036–4045.

Petrone, A., Battaglia, F., Wang, C., Dusa, A., Su, J., Zagzag, D., Bianchi, R., Casaccia- Bonnefil, P., Arancio, O., Sap, J., 2003. Receptor protein tyrosine phosphatase alpha is essential for hippocampal neuronal migration and long-term potentiation. EMBO J. 22, 4121–4131.

Ridley, A.J., Hall, A., 1992. The small GTP-binding protein rho regulates the assembly of focal adhesions and actin stress fibers in response to growth factors. Cell 70, 389–399.

Ridley, A.J., Paterson, H.F., Johnston, C.L., Diekmann, D., Hall, A., 1992. The small GTPbinding protein rac regulates growth factor-induced membrane ruffling. Cell 70, 401–410.

Roche, S., Koegl, M., Barone, M.V., Roussel, M.F., Courtneidge, S.A., 1995. DNA synthesis induced by some but not all growth factors requires Src family protein tyrosine kinases. Mol. Cell. Biol. 15, 1102–1109.

Sbalzarini, I.F., Koumoutsakos, P., 2005. Feature point tracking and trajectory analysis for video imaging in cell biology. J. Struct. Biol. 151, 182–195.

Solnica-Krezel, L., Eaton, S., 2003. Embryo morphogenesis: getting down to cells and molecules. Development 130, 4229–4233.

Solnica-Krezel, L., Stemple, D.L., Mountcastle-Shah, E., Rangini, Z., Neuhauss, S.C., Malicki, J., Schier, A.F., Stainier, D.Y., Zwartkruis, F., Abdelilah, S., Driever, W., 1996. Mutations affecting cell fates and cellular rearrangements during gastrulation inzebrafish. Development 123, 67–80.

Syverud, K., Chinga, G., Johnsen, P.O., Leirset, I., Wiik, K., 2007. Analysis of lint particles from full-scale printing trials. Appita J. 60, 286–290.

Tahinci, E., Symes, K., 2003. Distinct functions of Rho and Rac are required forconvergent extension during Xenopus gastrulation. Dev. Biol. 259, 318–335.

Tamura, K., Dudley, J., Nei, M., Kumar, S., 2007. MEGA4: Molecular EvolutionaryGenetics Analysis (MEGA) software version 4.0. Mol. Biol. Evol. 24, 1596–1599.

Thisse, C., Thisse, B., Schilling, T.F., Postlethwait, J.H., 1993. Structure of the zebrafish snail1 gene and its expression in wild-type, spadetail and no tail mutant embryos. Development 119, 1203–1215.

Tiran, Z., Peretz, A., Sines, T., Shinder, V., Sap, J., Attali, B., Elson, A., 2006. Tyrosine phosphatases epsilon and alpha perform specific and overlapping functions in regulation of voltage-gated potassium channels in Schwann cells. Mol. Biol, Cell.

Topczewski, J., Sepich, D.S., Myers, D.C., Walker, C., Amores, A., Lele, Z., Hammerschmidt,M., Postlethwait, J., Solnica-Krezel, L., 2001. The zebrafish

glypican knypek controls cell polarity during gastrulation movements of convergent extension. Dev. Cell 1, 251–264.

Unterseher, F., Hefele, J.A., Giehl, K., De Robertis, E.M., Wedlich, D., Schambony, A., 2004. Paraxial protocadherin coordinates cell polarity during convergent extension via Rho A and JNK. EMBO J. 23, 3259–3269.

van der Sar, A.M., Zivkovic, D., den Hertog, J., 2002. Eye defects in receptor proteintyrosine phosphatase alpha knock-down zebrafish. Dev. Dyn. 223, 292–297.

Veeman, M.T., Axelrod, J.D., Moon, R.T., 2003. A second canon. Functions andmechanisms of beta-catenin-independent Wnt signaling. Dev. Cell 5, 367–377.

von Wichert, G., Jiang, G., Kostic, A., De Vos, K., Sap, J., Sheetz, M.P., 2003. RPTP-alpha acts as a transducer of mechanical force on alphav/beta3-integrin-cytoskeleton linkages. J. Cell Biol. 161, 143–153.

Wada, H., Iwasaki, M., Sato, T., Masai, I., Nishiwaki, Y., Tanaka, H., Sato, A., Nojima, Y., Okamoto, H., 2005. Dual roles of zygotic and maternal Scribble1 in neural migration and convergent extension movements in zebrafish embryos. Development 132, 2273–2285.

Wallingford, J.B., Fraser, S.E., Harland, R.M., 2002. Convergent extension: the molecular control of polarized cell movement during embryonic development. Dev. Cell 2, 695–706.

Warga, R.M., Kimmel, C.B., 1990. Cell movements during epiboly and gastrulation in zebrafish. Development 108, 569–580.

Westerfield, M., 1995. The Zebrafish Book. University of Oregon Press, Eugene, Oregon.

Wienholds, E., Schulte-Merker, S., Walderich, B., Plasterk, R.H., 2002. Target-selected inactivation of the zebrafish rag1 gene. Science 297, 99–102.

Zeng, L., Si, X., Yu, W.P., Le, H.T., Ng, K.P., Teng, R.M., Ryan, K., Wang, D.Z., Ponniah, S., Pallen, C.J., 2003. PTP alpha regulates integrin-stimulated FAK autophosphorylation and cytoskeletal rearrangement in cell spreading and migration. J. Cell Biol. 160, 137–146.

Zhang, S.Q., Yang,W., Kontaridis, M.I., Bivona, T.G.,Wen, G., Araki, T., Luo, J., Thompson, J.A., Schraven, B.L., Philips, M.R., Neel, B.G., 2004. Shp2 regulates SRC family kinase activity and Ras/Erk activation by controlling Csk recruit-

ment. Mol. Cell 13, 341–355.

Zheng, X.M., Wang, Y., Pallen, C.J., 1992. Cell transformation and activation of pp 60c-src by overexpression of a protein tyrosine phosphatase. Nature 359, 336–339.

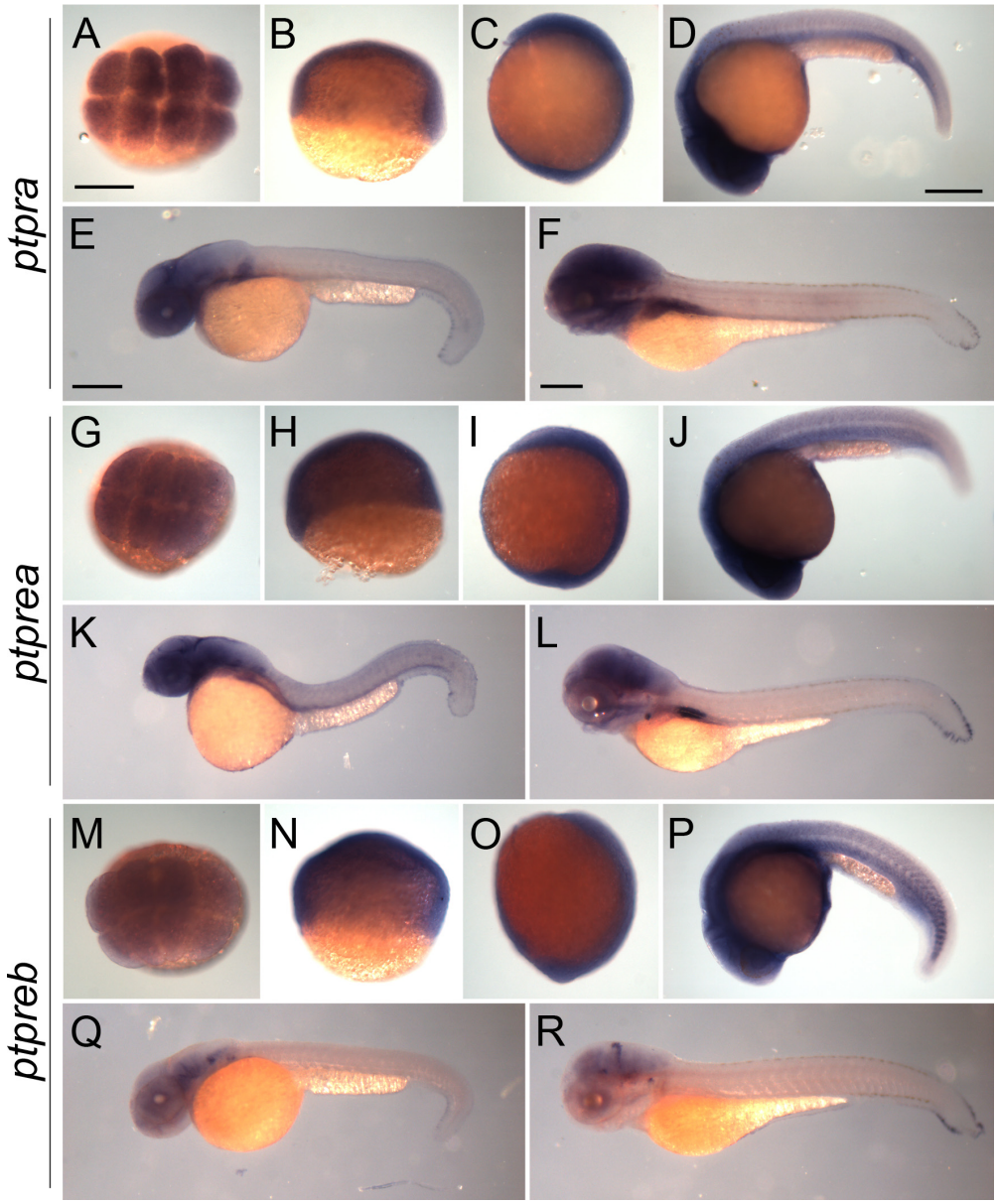

Fig. S1. *ptpra*, *ptprea* and *ptpreb* are ubiquitously expressed during early zebrafish development.
Wildtype zebrafish embryos were collected and fixed at 8 cell stage (A, G, M), 6 hpf (B, H, N), 1 somite stage (C, I, O), 24 hpf (D, J, P), 36 hpf (E, K, Q) and 72 hpf (F, L, R). Whole mount *in situ* hybridization was performed using probes targeting *ptpra* (A–F), *ptprea* (G–L) or *ptpreb* (M–R). Scale bars = 250 µm.

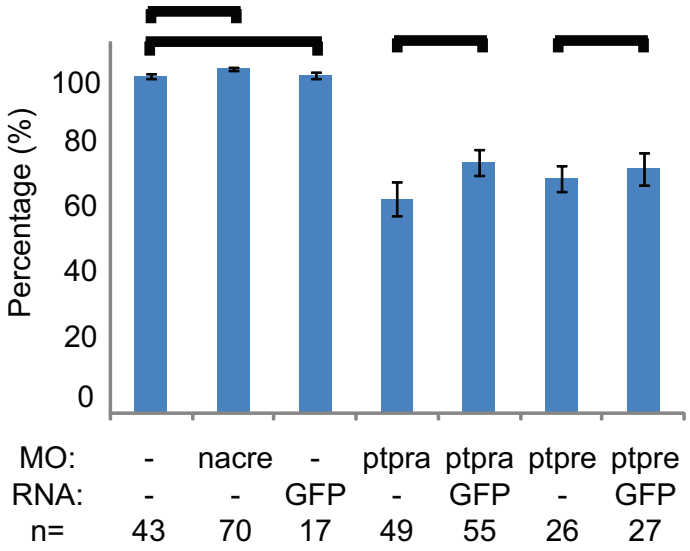

Fig. S2. Mock morpholino or RNA (co-) injections do not alter phenotype or length.
(A) Embryos were micro-injected at the 1-cell stage with either nacre morpholino, ptpra-MO, ptpra-MO and GFP RNA, ptpre-MO or ptpre-MO and GFP RNA. Non-injected embryos were taken as control. Embryos were grown to 2 dpf and pictures were taken. Tail lengths were determined using ImageJ software and compared to non-injected control. The tail lengths of the embryos are plotted as the average relative to non-injected control embryos. A Student t-test was performed between the non-injected control and nacre MO groups, the ptpra-MO and ptpra-MO/GFP RNA groups and the ptpre-MO and ptpre-MO/GFP RNA groups. No significant differences were found in response to GFP RNA co-injection ($P > 0.05$).